SOFTWOOD LOG SHAPE MODELLING WITH SHADOW SCANNERS

Jean-Pierre Mongeau

Mathematician
Forintek Canada Corp.
Université Laval
P.O. Box 2208, Québec
Canada, G1K 7P4

Robert Beauregard

Graduate Student
Département des sciences du bois
Université Laval
P.O. Box 2208, Québec
Canada, G1K 7P4

and

Thomas E. G. Harless

Sawmill Systems Software Scientist
Forintek Canada Corp.
Université Laval
P.O. Box 2208, Québec
Canada, G1K 7P4

(Received July 1992)

ABSTRACT

This paper describes and evaluates new and existing models for exterior log geometry. Compatibility with 1, 2, 3, and 4-axis shadow scanners determined which models were selected for evaluation. Models were considered for potential use in sawmilling process simulation and optimization. The accuracy evaluation compared models based upon lost and added fiber percentages. All models tended to overestimate log cross section area. Popular circular and elliptical models provided the poorest accuracy. Elliptical models used with 2-axis or 3-axis scanners generated up to 8% lost fiber and up to 15% added fiber. The 3-axis dyadic and Chaikin models provided the best overall performance: lost fiber under 3.5% and added fiber under 13%. Results from the evaluation recommend a 3-axis scanner system for automatic positioning and breakdown optimization. The small benefit obtained from 4-axis models does not justify their use. Other technologies are recommended where better accuracy is needed.

Keywords: Log model, scanning, mathematical representation, accuracy.

INTRODUCTION

It is well known that achieving maximum profitability with scanners in softwood sawmilling is linked to scanner accuracy, precision and resolution. However, it is equally true, if not equally obvious, that achieving this maximum also depends strongly on the accuracy of mathematical models representing logs during breakdown optimization.

Scanner accuracy has been defined as the difference between measured values and their corresponding real world values (Funck et al. 1989). Scanner precision is the repeatability of a given measurement. Resolution has been defined as the smallest detectable distance between two objects. By analogy, model accuracy, resolution, and precision may be of concern. For given input data, all model results

Wood and Fiber Science, 25(3), 1993, pp. 261–277

are perfectly reproducible, so precision is not an issue. Resolution is limited by computer hardware characteristics that favor no model. However, models may be distinguished by their geometrical accuracy, hence the opportunity for this research. For this study the differences between the real and the representation were collected as areas of lost and added fiber. Lost fiber was that part of the log not included in the model, and added fiber that part of the model not included in the log. Results of these measurements were always expressed as percentages of the actual cross-sectional area, i.e., lost fiber percent and added fiber percent (collectively referred to as fiber percentages or fiber measurements).

One can classify existing log models in three categories (Alleckson et al. 1980): cross section, whole log, and computer array. In the first category, logs are represented by a set of cross section models. A cross section model could be the best ellipse that fits the log cross section or a set of points chosen around the log cross section perimeter. In the second category, a log surface is represented by a function (cylinder, truncated cone) or by a set of functions. In the last category, logs are represented by a 3-dimensional array. Each element of this array represents a part of the log. A number contained in an array element identifies the type of wood contained in the associated part of the log, e.g., 0 for nothing, 1 for sound wood, 2 for a knot. This model could directly represent internal log defects.

Only a few examples of the computer array model have been reported (e.g., Harless 1990; Reynolds 1970). The large computer capacity (computer memory) needed to handle such models limits their uses. However, they were developed for studies in which internal log representation was needed, i.e., in hardwood sawing. Whole log models were chosen when computer efficiency was the primary concern (Maness and Adam 1991; Hitrec et al. 1990; Lewis 1985b; Geerts 1984). On the other hand, for studies in which external shape accuracy was the first concern, cross section models were chosen (Zeng 1991; Sampson 1990; Leban and Duchanois 1990; Occena and Tanchoco 1988; Todokori 1988; Drake and Johansson 1985).

Generally speaking, scanners gather data describing log cross-sectional perimeters. Association of these cross sections permits reconstruction of the log shape. Thus log model accuracy is associated with cross section model accuracy. This research studied cross section model accuracy rather than log model accuracy.

Cross-sectional models may be classified as either functional or set-of-points. Functional models include circular and elliptical models. Set-of-points include Chaikin's Interpolation and Dyadic Interpolation models.

Earlier studies described volume yield losses resulting from specific models (Moen 1991; Rickford 1989) and another determined volume yield loss due to scanner error (Lewis 1985a). No study has yet presented a systematic evaluation and comparison of geometrical models used for softwood sawmilling simulation and optimization.

A link exists between scanner and log model performance. Model accuracy depends partly upon the quantity and quality of data gathered by a scanner, but part of the error arises solely from the model. Infinitely increasing scanner accuracy could not infinitely increase model accuracy. This study evaluated models associated with shadow scanners (light curtain scanner), which are widespread in eastern Canada softwood sawmills. Some models (Chaikin and dyadic) could be used with other types of scanners, e.g., laser, microwave.

Accuracy evaluation becomes meaningful after analyzing a study made by D. W. Lewis (Lewis 1985a). He showed in a study using a truncated cone geometrical model that an error of ± 2.5 mm (0.1 inch) for a diameter measurement generated volume yield losses between 2.6% and 9.8% for a 2.44-m-long and 20.3-cm-wide log. Diameter measurement error is a scanner error. Applying this result to model error, for the same log, an error of ± 2.5 mm in the diameter measurement yields a range of $\pm 1\%$ in the percentage of well-represented fiber. For a truncated cone log, a diameter overestimate produces added fiber percentage, but no lost fiber. Conversely, a diameter underestimate produces lost fiber, but no added fiber. For true log shapes, lost fiber and added fiber are present on the same cross section. The effect of the underestimate (2.6% volume yield lost for 1% lost fiber) and the effect of overestimate (9.8% volume yield lost for 1% added fiber) are present together. Because of the real log shapes used in this study, the resulting yield losses are only indicative, but Lewis's study emphasized the importance of accuracy in sawing optimization. Increasing accuracy by 1% provided valuable yield improvement. The Lewis study needs to be performed on true shape logs, where both lost and added fiber are present, in order to evaluate the true value of losses.

The next section presents mathematical equations employed by different models used with shadow scanners. The third section presents the materials and methods used to evaluate model accuracy. The fourth section presents evaluation results.

MODEL DESCRIPTIONS

This section describes two circular, two elliptical, Chaikin's and dyadic models. Circular models and the first elliptical model are well known and widely used. The second elliptical model has been partially developed in the literature (Rickford 1987). The two other models are presented for the first time for this application.

Circular models

The circle is defined by the set-of-points (x,y) that fulfills the following equation:

$$(x - c_x)^2 + (y - c_y)^2 = r^2 \qquad (1)$$

where r is the radius and (c_x, c_y) the center of the circle. A one-axis shadow scanner (Fig. 1) is commonly used to find values for the radius and center. Figure 2 illustrates another type of 1-axis scanner that improves model accuracy, as will be seen later.

Equations (2) and (3) provide radius, r, and

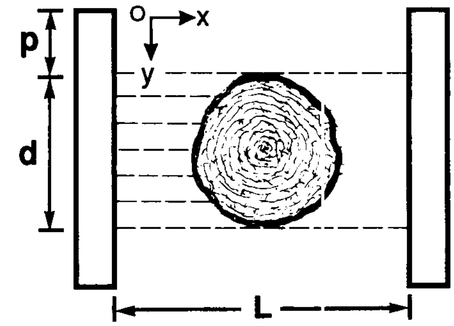

FIG. 1. Horizontal 1-axis scanner: The transmitter on the left emits an infrared ray curtain. The rays that narrowly miss the log are referred to as tangent rays, and are those that determine values for variables p (position along the receiver) and d (diameter on the receiver).

center (c_x, c_y), for a circle. For a horizontal scanner (Fig. 1):

$$(c_x, c_y) = \left(\frac{L}{2}, p + \frac{d}{2}\right), \qquad r = \frac{d}{2} \qquad (2)$$

The value for c_x can only be assumed to be midway between transmitter and receiver. The true center x-coordinate is unknown. For a 45° scanner (Fig. 2):

$$(c_x, c_y) = \left(\sqrt{2}\left(\frac{E}{2} - p - \frac{d}{2}\right) + \right.$$
$$\left. + \frac{E - d}{2}, \frac{E - d}{2}\right), \qquad r = \frac{d}{2} \qquad (3)$$

where d, p, and E are the measured section diameter and position, and the width of the scanner.

Elliptical models

The ellipse is defined by the set-of-points that fulfils the following equation:

$$\left(\frac{x - c_x}{d_x}\right)^2 + \left(\frac{y - c_y}{d_y}\right)^2 = 1 \qquad (4)$$

where (c_x, c_y), d_x and d_y are, respectively, the center, the x diameter, and the y diameter. This study considered both 2-axis and 3-axis scanner systems. Figures 3 and 4 illustrate these two systems. The 3-axis system allows for rotated ellipses (major and minor axes not parallel to coordinate axes), thereby improving

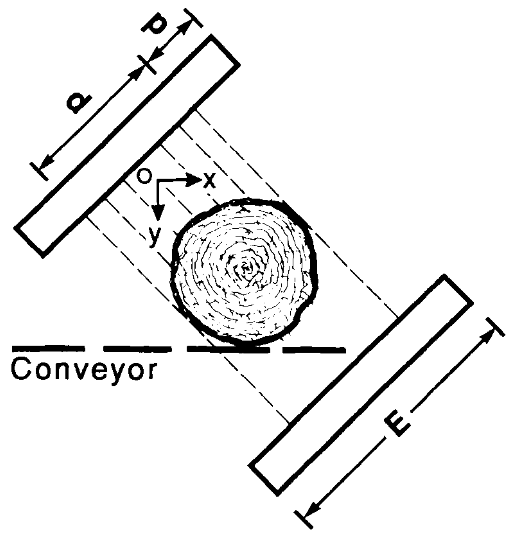

FIG. 2. 45° 1-axis scanner: The position of the conveyor adds an additional piece of information useful for locating the cross section center.

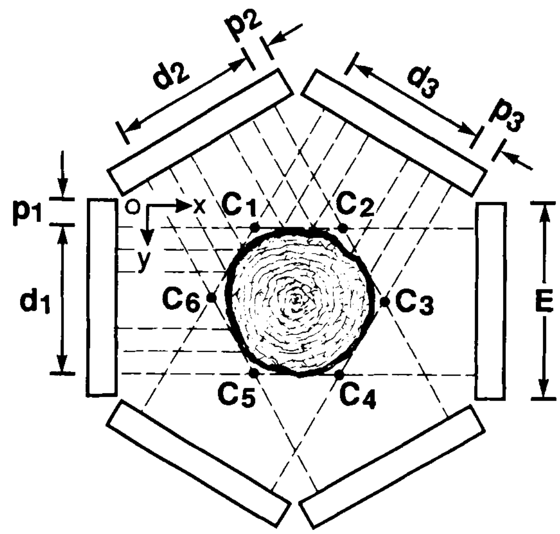

FIG. 4. 3-axis scanner: These scanners determine three sets of values for p and d, and coordinates for six tangent ray intersection points.

model accuracy. The following equations determine ellipse parameters. For a 2-axis scanner (Fig. 3):

$$(c_x, c_y) = \left(E - p_2 - \frac{d_2}{2}, p_1 + \frac{d_1}{2}\right),$$
$$d_x = d_2, \qquad d_y = d_1 \tag{5}$$

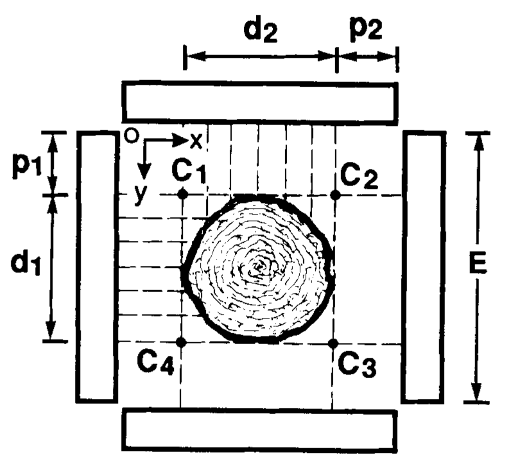

FIG. 3. 2-axis scanner: Different values for p and d are determined for each pair. The resulting values (p_1, p_2, d_1, d_2) are used to determine the intersection points C_1, C_2, C_3 and C_4 of the tangent rays.

where p_i, d_i, E are defined according to Fig. 3. For a 3-axis scanner, first (Fig. 4), define the following five values r, s, t, u and v as:

$$r = \frac{d_3^2 + d_2^2 - \frac{d_1^2}{2}}{6}, \qquad s = \frac{d_1^2}{4},$$
$$t = \frac{d_3^2 - d_2^2}{4\sqrt{3}}, \qquad u = (r - s)^2 + 4t^2,$$
$$v = r + s \tag{6}$$

If: $v > \sqrt{u}$ then define a and b as:

$$a = \sqrt{\frac{v + \sqrt{u}}{2}}, \quad b = \sqrt{\frac{v - \sqrt{u}}{2}} \tag{7}$$

otherwise:

$$a = \sqrt{\frac{v + \sqrt{u}}{2}}, \qquad b = a \tag{8}$$

Then the diameters are:

$$d_x = 2a, \qquad d_y = 2b \tag{9}$$

Equations (10) provide the cosine and the sine of the angle θ; if a = b, then $\cos(\theta) = 1$ and $\sin(\theta) = 0$; otherwise:

$$\cos(\theta) = \sqrt{\frac{sb^2 - ra^2}{b^4 - a^4}},$$

$$\sin(\theta) = \sqrt{\frac{rb^2 - sa^2}{b^4 - a^4}} \qquad (10)$$

If: $d_3 < d_2$, then multiply s by -1. The ellipse center is given by:

$$c_x = \frac{2(E - p_2) - d_2 + p_1 + \frac{d_1}{2}}{\sqrt{3}} + \frac{1 - \sqrt{3}}{2}E,$$

$$c_y = p_1 + \frac{d_1}{2} \qquad (11)$$

The preceding equations apply if an only if the three intersection points c_1, c_2, and c_3 of the middle axes are equal (Fig. 5), i.e., there is one intersection point. The following paragraphs provide a technique that permits finding the ellipse for every set of measurements.

In this technique, the measured diameters are changed in order to provide a new set of measurements in which the three middle axes have the same intersection point. Define c as the center of the triangle formed by the three intersection points c_1, c_2 and c_3 of the middle axes (Fig. 5). Then:

$$c = \frac{c_1 + c_2 + c_3}{3} \qquad (12)$$

where $c = (c_x, c_y)$ and $c_i = (c_{xi}, c_{yi})$, $i = 1, 2, 3$. Take c as the center of the ellipse. The three diameters become:

$$d_i' = d_i - \sqrt{(c_{xi} - c_x)^2 + (c_{yi} - c_y)^2}, \quad i = 1, 2, 3 \qquad (13)$$

The coordinates of points c_1, c_2 and c_3 are computed with by Eqs. (14) and (15). Define A, u_1, u_2, and u_3 as:

$$A = E\frac{1 - \sqrt{3}}{2}, \qquad u_i = E - p_i - d_i, \quad i = 1, 2, 3 \qquad (14)$$

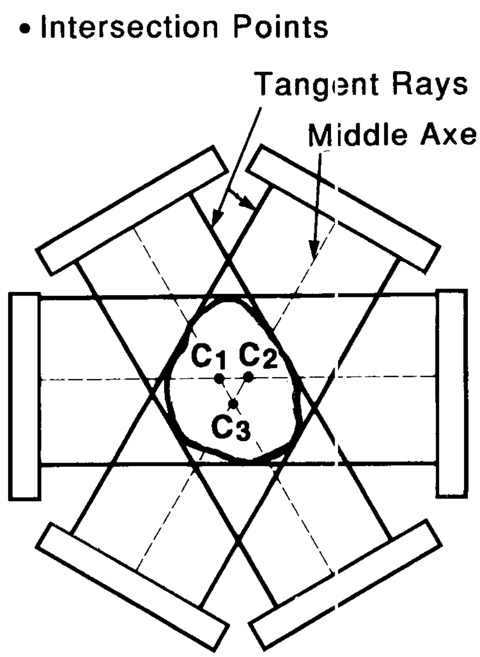

FIG. 5. Tangent rays of the 3-axis scanner: The tangent rays determine 3 mid-axes that intersect at points C_1, C_2 and C_3.

then:

$$c_1 = \left(\frac{2(E - u_1 + 2u_2 + d_2) - d_1}{2\sqrt{3}} + A,\ E - u_1 - \frac{d_1}{2}\right)$$

$$c_2 = \left(\frac{2(2u_3 + d_3 + u_1) + d_1}{2\sqrt{3}} + A,\ E - u_1 - \frac{d_1}{2}\right) \qquad (15)$$

$$c_3 = \left(\frac{2u_2 + d_2 + 2u_3 + d_3 + E}{2\sqrt{3}} + A,\ \frac{E + d_3 - d_2}{2} + u_3 - u_2\right)$$

Set-of-points models

"Set-of-points" models represent log cross sections by a set of tangent points rather than equations. Starting from points gathered by the scanner, the model builds the section representation with the number of points requested by the user. Before describing these models, let us present tangent ray intersection point equations for 2-axis, 3-axis and 4-axis scanners. Intersection points c_1, c_2, c_3 and c_4 for a 2-axis scanner (Fig. 3) are computed from:

$$\begin{aligned} c_1 &= (E - p_2 - d_2, p_1), \\ c_2 &= (E - p_2, p_1), \\ c_3 &= (E - p_2, d_1 + p_1), \\ c_4 &= (E - p_2 - d_2, d_1 + p_1) \end{aligned} \tag{16}$$

where p_i, d_i, E are defined in Fig. 3. Intersection points c_1, c_2, c_3, c_4, c_5 and c_6 for a 3-axis scanner (Fig. 4) are computed from:

$$\begin{aligned} c_1 &= \left(\frac{2u_3 + u_1 + d_1}{\sqrt{3}} + A, p_1\right) \\ c_2 &= \left(\frac{p_1 + 2(E - p_2)}{\sqrt{3}} + A, p_1\right) \\ c_3 &= \left(\frac{5E - 2p_2 - 2p_3}{2\sqrt{3}} + A, \frac{E}{2} + p_2 - p_3\right) \\ c_4 &= \left(\frac{u_1 + 2(E - p_3)}{\sqrt{3}} + A, p_1 + d_1\right) \\ c_5 &= \left(\frac{p_1 + d_1 + 2u_2}{\sqrt{3}} + A, p_1 + d_1\right) \\ c_6 &= \left(\frac{E + 2(u_3 + u_2)}{2\sqrt{3}} + A, \frac{E}{2} + u_3 - u_2\right) \end{aligned} \tag{17}$$

where u_i, p_i, d_i and E were defined in Fig. 4 and Eq. (14).

Intersection points c_1, c_2, c_3, c_4, c_5, c_6, c_7 and c_8 for a 4-axis scanner are computed from (18):

$$\begin{aligned} c_1 &= \left(p_1 + \frac{E}{\sqrt{2}} - \sqrt{2}p_2, p_1\right) \\ c_2 &= \left(E - p_3, \left(1 - \frac{1}{\sqrt{2}}\right)E - p_3 + \sqrt{2}p_2\right) \\ c_3 &= \left(E - p_3, \frac{E}{\sqrt{2}} + p_3 - \sqrt{2}p_4\right) \\ c_4 &= \left(\frac{\sqrt{2} + 1}{\sqrt{2}}E - \sqrt{2}p_4 - p_1 - d_1, p_1 + d_1\right) \\ c_5 &= \left(p_1 + d_1 + \frac{E}{\sqrt{2}} - \sqrt{2}(p_2 + d_2), p_1 + d_1\right) \\ c_6 &= \left(E - p_3 - d_3, \frac{\sqrt{2} - 1}{\sqrt{2}}E - p_3 - d_3 + \right. \\ &\qquad \left. + \sqrt{2}(d_2 + p_2)\right) \\ c_7 &= \left(E - p_3 - d_3, \frac{E}{\sqrt{2}} - \sqrt{2}(p_4 + d_4) + \right. \\ &\qquad \left. + p_3 + d_3\right) \\ c_8 &= \left(\frac{\sqrt{2} + 1}{\sqrt{2}}E - \sqrt{2}(d_4 + p_4) - p_1, p_1\right) \end{aligned} \tag{18}$$

where E, p_i and d_i are defined in a fashion comparable to those for a 3-axis scanner.

Chaikin's interpolation

The general methodology of Chaikin's interpolation starts with a coarse polygonal representation for a log cross section, then improves its representation by cutting corners (Fig. 6) (Chaikin 1974). Step 1 illustrates an initial ABCD polygon (ABCD was collected from a 2-axis scanner in this example). The starting points are the intersection points of the tangent rays of the 2-, 3- or 4-axis scanner. Step 2 computes intermediary points A′, B′, A″ and B″. Step 3 rounds the polygon corners by deleting A, B, C, and D points. This process repeats in order to produce the desired number of points around the cross section.

Between adjacent points A and B, compute new points A′ and A″ using the following equations.

$$A' = \frac{3A}{4} + \frac{B}{4}, \qquad A'' = \frac{A}{4} + \frac{3B}{4} \tag{19}$$

Other new points are computed similarly.

Dyadic interpolation

This technique uses a new interpolation process presented by S. Dubuc (Dubuc 1986; Mongeau 1990). Rather than rounding a polygon, the method starts with a polygon approx-

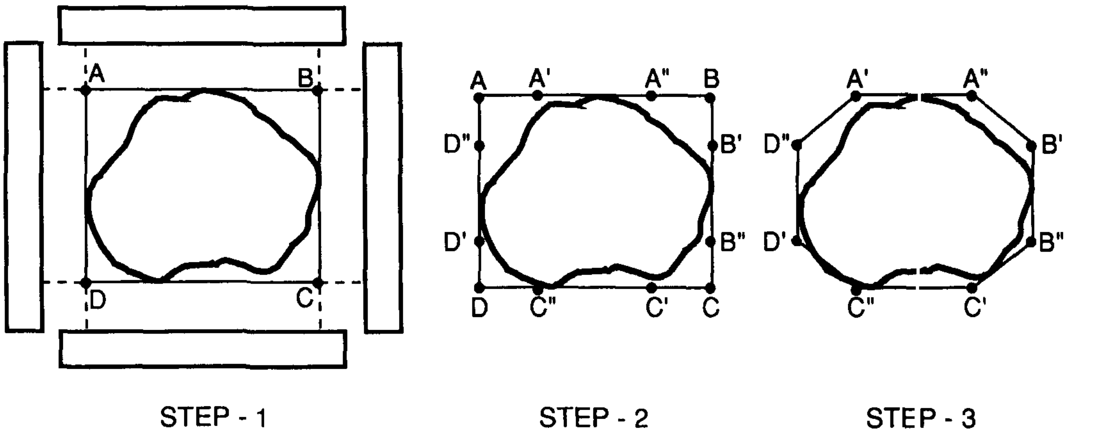

FIG. 6. Chaikin's interpolation process starts with a rectangle determined by the intersection points of tangent rays. In STEP 2, two new points are set on each side based on the coordinates of side end-points. The old points are discarded and a new representation determined as shown in STEP 3.

imatively inscribed within the log cross section and then enlarges it by adding sides (Fig. 7). Step one sets the initial polygon. Starting points are the middle points of the segments defined by the intersection points of the tangent rays of the 2-, 3- or 4-axis scanner (2-axis scanner is shown on Fig. 7). The middle points are chosen to approximate the tangent points of the tangent rays. Step two computes intermediary point A′, B′, C′ and D′. Step three builds a new polygon with all points. The process repeats in order to provide the desired number of points. In general, for each set of 4 consecutive points in a polygon (with N points), P_{i-1}, P_i, P_{i+1}, and P_{i+2}, i = 1, N, a point P′ is added between P_i and P_{i+1} computed as:

$$P' = -\frac{P_{i-1}}{16} + \frac{9P_i}{16} + \frac{9P_{i-1}}{16} - \frac{P_{i+2}}{16} \tag{20}$$

then:

$$A' = -\frac{D}{16} + \frac{9A}{16} + \frac{9B}{16} - \frac{C}{16} \tag{21}$$

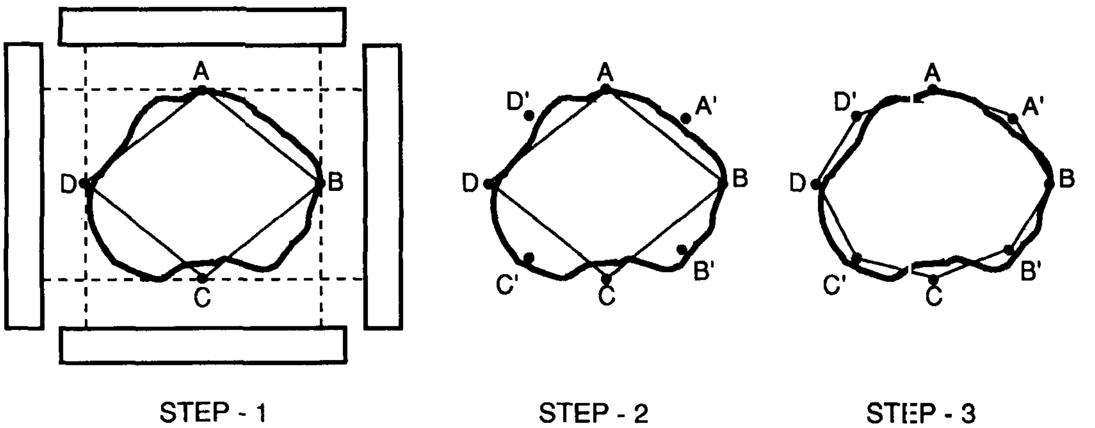

FIG. 7. The dyadic interpolation process starts with a polygon determined by connecting the mid-points between the intersection points of tangent rays. In STEP 2, one new point is set based on the coordinates of each set of 4 adjacent points. The new points are added to the old and a new representation determined as shown in STEP 3.

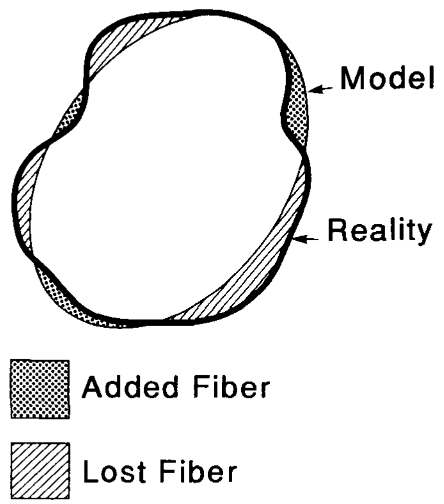

FIG. 8. An irregular log cross section is shown with its ellipse representation. Areas of fiber lost and added by the ellipse are identified.

and so on. For both Chaikin's and dyadic models, 48 and 64 points per cross section were computed for the 3- and 4-axis scanners, respectively.

MATERIALS AND METHODS

Three balsam fir stems (*Abies balsamea* (L.) Mill.), felled 90 km north of Québec City, in the Parc des Laurentides, were cut into at least 20 cross sections each. These stems had big end diameters and lengths of 15-cm, 7.8-m; 19.5-cm, 11-m; and 16.5-cm, 5.6-m, respectively. Cross sections were not equally spaced along the stem. Five cross sections were cut at each of the following locations: stump, breast height, mid-height and "top" (where stem diameter became smaller than 10 cm (4 inches)). Finally, eleven additional cross sections were cut at sweepy points along one stem for a total of 71 cross sections.

The cross section shapes were digitized with a Microtech 300-Z scanner at a resolution of 39 dots per centimeter (99 dots per inch). Each digitized cross section was drawn on a 640 × 480 pixel graphical adapter with a resolution of 26 dots per centimeter (66 dots per inch) in 36 evenly distributed rotational orientations starting from a random initial position. The 36 orientations spanned 45° with increments of 1.25°. A higher resolution on the Microtech scanner permitted rotation of the digitized cross sections without loss of precision. Shadow scanning was simulated within the graphical adaptor pixel grid at the following angles: 0, 45, 60, 90, 120, and 135 degrees. Each scan yielded one position and one diameter. measurements at 0° and 45° provided horizontal 1-axis and 45° 1-axis scanner data, respectively. Sets of measurements at 0° and 45°; 0°, 60°, and 120°; and 0°, 45°, 90°, and 135° provided, respectively, 2-, 3- and 4-axis scanner data. These different measurement sets were chosen to reflect existing scanners offered by manufacturers. The 90° 1-axis model provided results similar to that of the 45° 1-axis scanner and is not presented. Another strategy may suggest testing other sets of orientations. This study tested only scanner heads evenly distributed around the logs. For each cross section and for each orientation, lost fiber percentage and added fiber percentage were computed (Fig. 8).

EVALUATION METHODS

Variation in cross-sectional shape both within and between logs is large, and the sample collected was too small to provide representative, physically significant results. Consequently, rather than perform a complex statistical analysis, a simpler set of comparisons was made with the means and ranges of the fiber area measurements.

The experiment performed involved processes—tracing log cross sections and their subsequent digitization and simulated scanning—that produced measurements (the physical tracing, a set of digitized points, and diameter measurements) that, like all data, are not exact and may introduce uncertainty into the added fiber and lost fiber results. Note that the final determination of these areas involved simply counting pixels in the graphical adaptor and was performed exactly. Uncertainty, as conceived by, among others, Coleman and Steele (1989), is the "degree of goodness" of a measurement or experimental result. When a formula employs experimentally determined values, the uncertainty of the result can be related to the uncertainty of individual input variables with the general uncertainty expression (Coleman and Steele 1989).

For each section orientation in the graphical adaptor, the Microtech data are rotated. During the process of rotation, a new set of pixels was chosen. Locations of each pixel, for each orientation, required rounding the digitized point coordinates to new integral values. This rounding created a measurement uncertainty for each coordinate pair of one-half pixel. Given that the simulated scanning shadow lines are tangent at 2 independent points, the uncertainty in the diameter measurement was computed by plugging the standard 2-dimensional distance equation into the general uncertainty expression. The diameter uncertainty was 0.707-pixels. The uncertainty in the position measurements was 0.500-pixels, i.e., the error in specific pixel coordinates.

Each model uses the diameter and position measurements in different ways, and each will have a different fiber measurement uncertainty. Furthermore, since fiber measurements are determined numerically (counting pixels in the graphical adaptor), the uncertainty in these measurements can be determined only by perturbing (one at a time) model parameters by their respective uncertainties for (a sample of) actual representations and observing how the "perturbed" fiber measurements differ from the original. The uncertainty would then be computed as:

$$U_R = \sqrt{\Sigma\,(E_{mi} - E_0)^2} \tag{22}$$

where

- U_R = uncertainty in fiber error measurement (lost or added) for particular scanner system,
- E_0 = fiber error with original scanner measurements (p and d),
- E_{mi} = fiber error with only the i-th scanner measurement perturbed,
- N = number of scanner measurements (N = 2, 4, 6, 8 for 1, 2, 3, 4-axis scanners, respectively).

The uncertainties of a sample of cross sections and orientations were collected and averaged to produce, for each scanner system, the uncertainties for lost and added fiber for a cross section at one orientation. The uncertainties for added fiber varied between 1.4% for the circle 45-degree scanner and 0.45% for the Dyadic 4-head scanner. Uncertainties for lost fiber varied between 1.10% for the ellipse 3-head scanner to 0.17% for the Chaikin 4-head scanner. The range of fiber errors (among 36 orientations of a cross section) computed has an uncertainty of 1.414 times the single uncertainty of the single measurement uncertainty. The uncertainty of a simple average of M values is the product of the single measurement uncertainty and the inverse square root of M. For the 45-degree circle scanner system (this model provided the maximum uncertainty), the uncertainty of the average of 71 added fiber error ranges was 0.23 ($1.414 \times 1.4/\sqrt{71}$); and the uncertainty of the average added fiber error over 36 orientations was also 0.23 ($1.4/\sqrt{36}$). For the sake of simplicity for all model comparisons, differences higher than 0.23 will be regarded as real experimental differences. The approach compared models with their best and worst performances. Accuracy was evaluated with regard to consistency, flexibility, and overall exactness.

Ideally, representations of a cross section at different orientations should differ only by an angle of rotation. A perfectly consistent model would provide such representations. To gauge this characteristic, the variation of fiber measurements due to cross section orientation was observed. For each cross section and model, the fiber percentages were computed for each of the 36 orientations, and from these ranges of both fiber percentages were computed. For a model, the mean of the 71 ranges for each fiber percent was computed. This mean represents overall model sensitivity to section orientation. Consistent models should have small ranges for fiber percentages. Models having

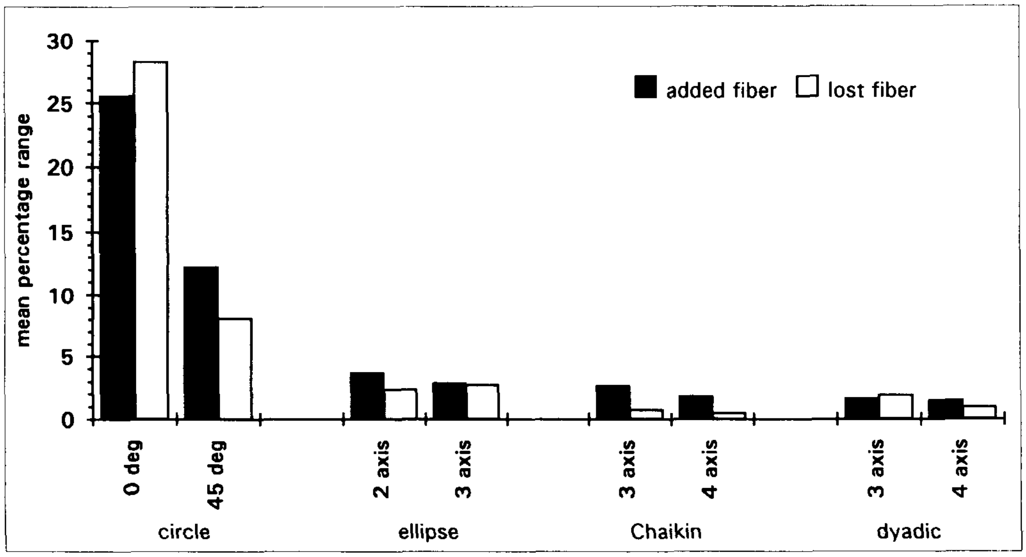

FIG. 9. The consistency comparison is based upon the range (maximum less minimum) of error measurements among different log orientations. This range indicates error sensitivity to orientation. Smaller ranges are preferred. A mean range was determined over all sections for each model and number of axes.

large ranges cannot provide a consistent representation independent of the cross section orientation.

Flexible models conform equally well to different cross-sectional shapes. With respect to tree stems, cross-sectional shape varies considerably from stump to top; thus the appropriateness of graphing fiber percentages versus stem position for each model and log. A flexible model would generate the same fiber percentages for each stem position. For each cross section, the mean of the 36 values for each fiber percentages represented a single stem position. Averaging the fiber percentages at the same position in different logs is not appropriate as a measure of flexibility. Choosing an accurate model for stump cross sections is important for small log processing.

A perfectly exact model describes a cross section without error. In this evaluation, that error was measured as added fiber and lost fiber. As with the flexibility measure, for each model and cross section, the average of each fiber percentage for all orientations was considered. The overall exactness of a model was represented by the maximum and minimum of each fiber percentage for all logs and all regular cross sections. Excluding irregular cross sections (those including part of branch or scanner error) permits a fairer comparison between models by deleting extreme cases. Computer automated systems usually include data filters that eliminate scanner reading error and irregular cross section shapes in order to provide smoother data to optimization algorithms. Consequently, these graphs present pooled means useful to globally compare models over smoothed data.

CONSISTENCY COMPARISONS

For a comparison of consistency, Fig. 9 presents a graph illustrating each model's fiber measurement ranges. The lower the range, the more consistent is the model.

Generally speaking, the horizontal circular model was extremely inconsistent. Variations over 25% of added and lost fiber were found. By simply rotating the scanner to 45°, the range was reduced to 12.5% added fiber and 9% lost fiber. This great improvement came from better detection of log position; the location of the x-coordinate was computed rather than assumed. The horizontal 1-axis scanner is commonly used for volume computation and sorting only. Still, the second circular model may not be regarded as consistent enough for log breakdown optimization.

Elliptical models provided distinctly more consistent results. The 2-axis model ranges equalled 2.5% lost fiber and 3.5% added fiber. The 3-axis ranges were both approximately 3%.

In general, a shadow scanner can be thought of as sampling the perimeter of a section. A one-axis scanner samples the positions of 2 points on the perimeter. Given the irregularity of log cross sections and such a small sample, high variation, therefore inconsistency, was expected and realized. The 45-degree scanner explicitly samples the cross section at as many points as the horizontal scanner, but since the nonhorizontal (45-degree) shadow lines imply a set of horizontal lines (also separated by the scanned diameter) that bound the section, both coordinates of the center could be computed from scanner data. One of these lines is defined by the conveyor position. Consequently, both center coordinates vary with section orientation, as opposed to only c_y with the horizontal scanner, thereby producing better consistency for the 45-degree scanner. A two-axis scanner samples 4 point locations on each cross section, so any highly irregular point is less dominant, hence less variation (range), and better consistency. This improvement was realized by the elliptical 2-axis scanner system. Results for the 3-axis scanner (ellipse model) and 4-axis scanner (other models) show the decreasing value of a larger sample, at least with respect to consistency.

Ranges were limited to 2% lost fiber and 1.5% added fiber for dyadic models and to 1% lost fiber and 3% added fiber for Chaikin's models. Set-of-points models provided greater consistency than functional models.

FLEXIBILITY COMPARISONS

The variation of fiber measurements due to stem location was studied stem by stem. For the sake of brevity, results from only selected cross sections of one log are presented. However, graphs of Figs. 10 and 11 are representative of those obtained with other stems. Cross section "top 3" included part of branch or scanner error and was excluded from the analysis.

Graphs of Fig. 10 present the mean added and lost percentages obtained with function type models: the 1-axis circle, the 2- and 3-axis ellipse. The horizontal 1-axis circular model always generated more than 10% lost or added fiber, while the 45° 1-axis model exhibited a more satisfactory behavior. The 45° 1-axis circular model, and the 2- and 3-axis elliptical models were less accurate at the stump cross sections than for the rest of the stem. In the case of the 45° 1-axis circle, lost fiber was less than 8% for the stem, and less than 5% with stump excluded, while added fiber was less than 18% for the stem, and less than 6% for the stem excluding the stump. The 2- and 3-axis scanners provided similar variation between stem sections (excluding stump) and stump sections. For the 2- and 3-axis elliptical models, lost fiber measurements were, respectively, less than 8% and 5% for the stem, less than 5% excluding stump, while added percentages were less than 12% and 10% for the stem, and less than 5% and 3% excluding stump.

Graphs in Fig. 11 present results obtained with set-of-points models. The 3-axis and 4-axis Chaikin's interpolation generated less than 1.1% lost fiber for the stem, and less than 0.5% stump excluded, while providing less than 13% and 5% added fiber for whole stem and stem excluding stump, respectively. The 3-axis dyadic interpolation presented less than 3.5% and 2.5% lost fiber for the entire stem and without stump, respectively. Added fiber was less than 11% and 3%, respectively. Finally, 4-axis dyadic interpolation presented 1.4% and 0.8% lost fiber with stump and without stump, and 10% and 3% added fiber with stump and without stump, respectively.

Circular models excepted, models were quite comparable with respect to added fiber measurements. Some maximums were higher than others, but their flexibility was similar. Added fiber increased to approximately 7% at stump.

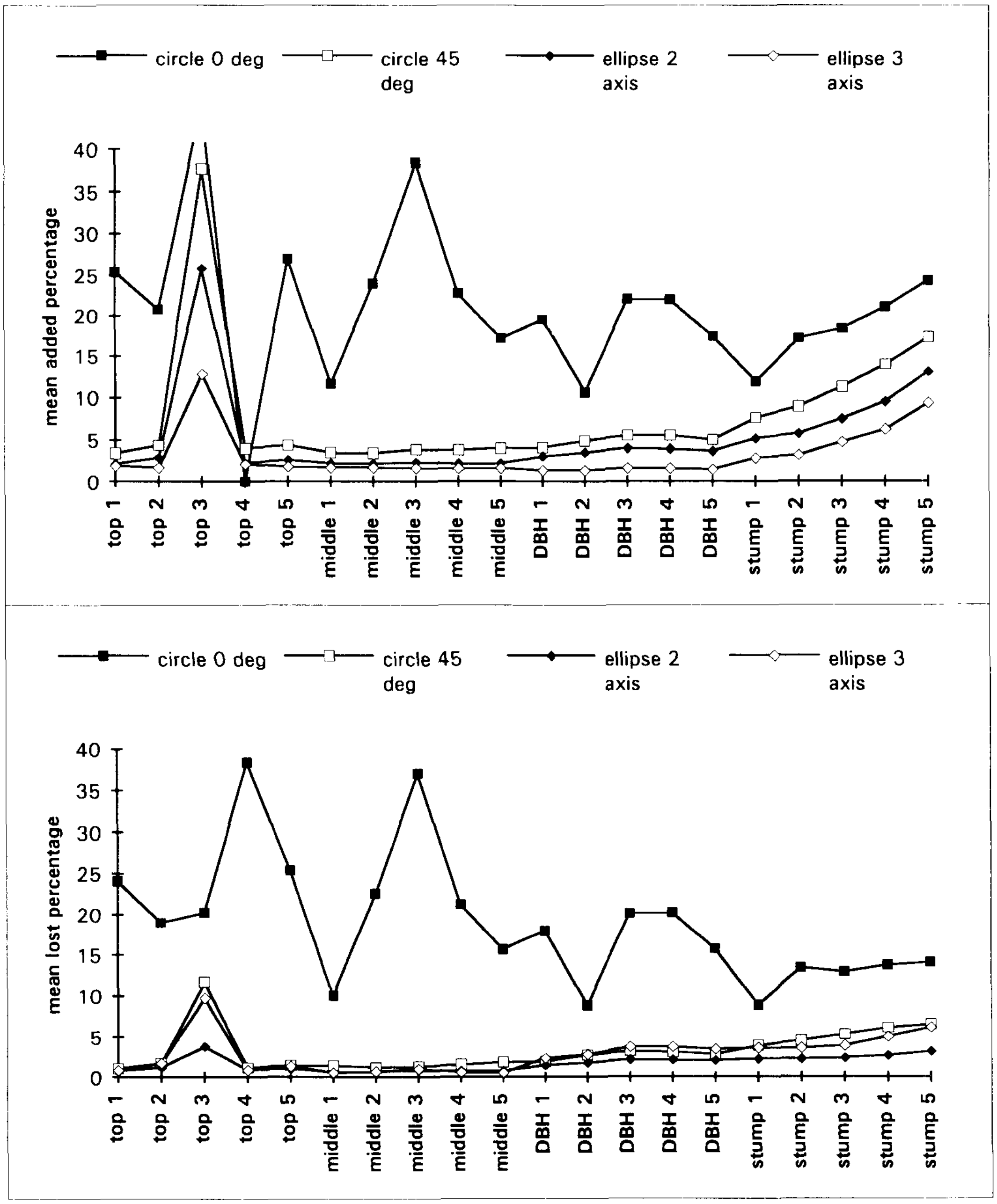

FIG. 10. Mean lost and added fiber errors (over all orientations) are shown for one log for each section and both functional models. For a single model, the variability in these mean errors indicates flexibility of the model for representing different section geometries. Less variability is preferred.

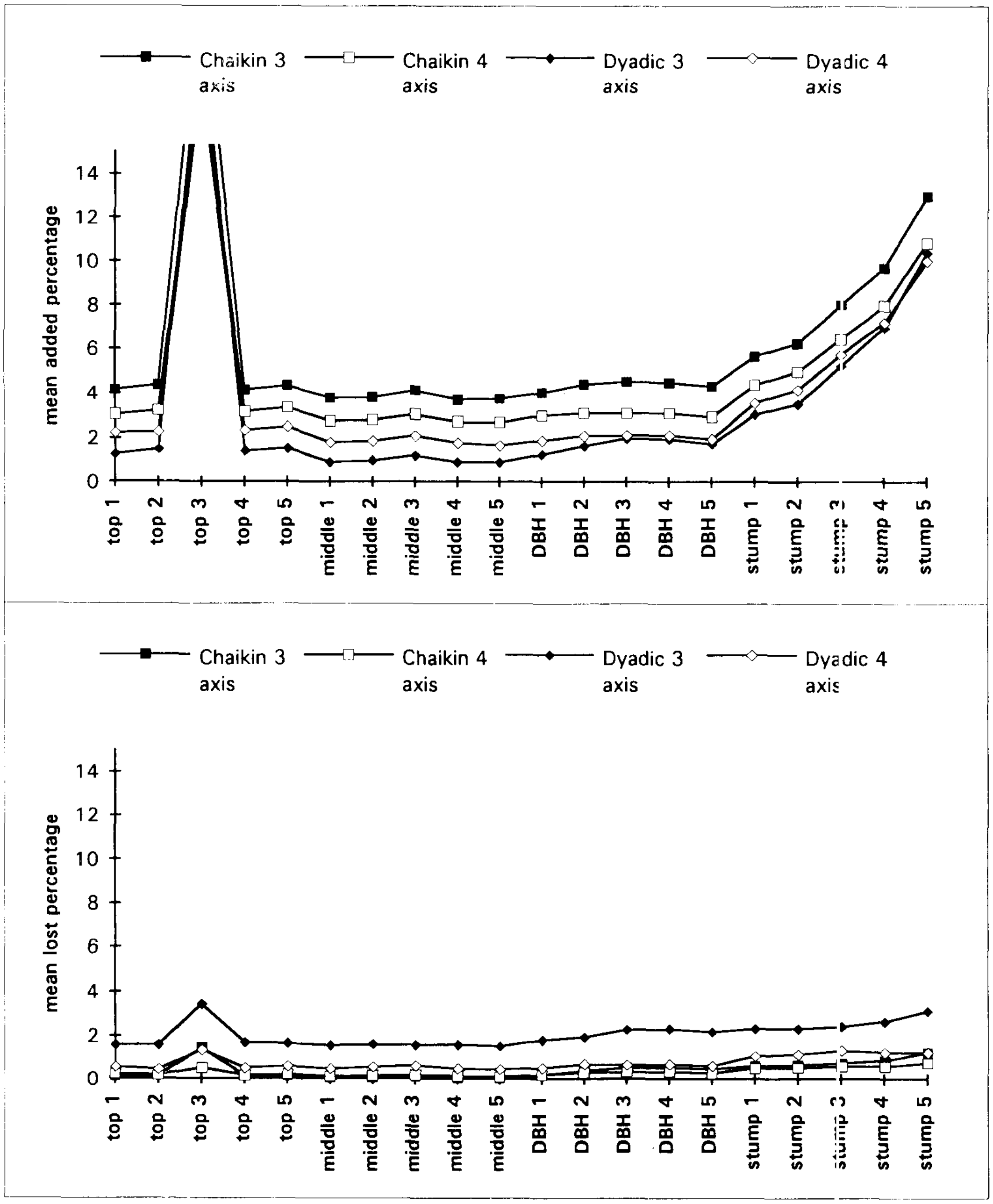

FIG. 11. Like results in Fig. 10, the degree of flexibility was also observed for set-of-points models.

Lost fiber increased 1% to 3% at stump. Added fiber measurements were less flexible than lost percentages. Set-of-points model flexibility with respect to lost percentages was slightly better than that of the functional models.

EXACTNESS COMPARISONS

Figure 12 presents examples of how fiber measurements varied with orientation for one particular cross section with two different models. For overall comparisons of exactness,

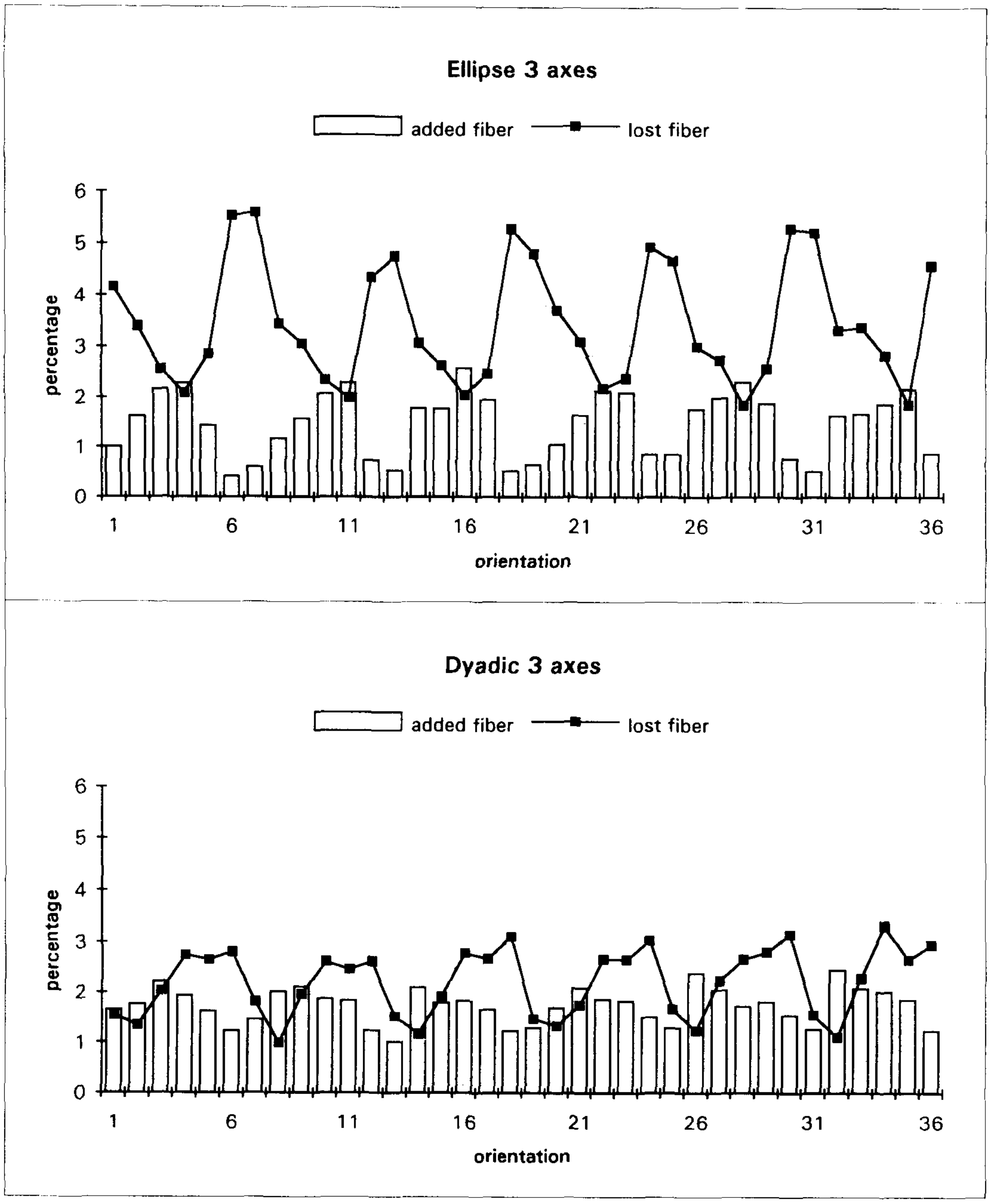

FIG. 12. For two different models, graphs present fiber measurements for one cross section at each orientation (spanning 0° to 360°).

Fig. 13 shows ranges of the mean fiber measurements of all cross sections (excluding irregular ones). The inexactness of circular models is now evident. Fiber percentages higher than 15% were found. Elliptical models generated less than 15% added fiber and less than 8% lost fiber. Elliptical 3-axis models provided less than 11% added fiber and less than 8% lost fiber. It provided more exact results than any other functional model for both fiber mea-

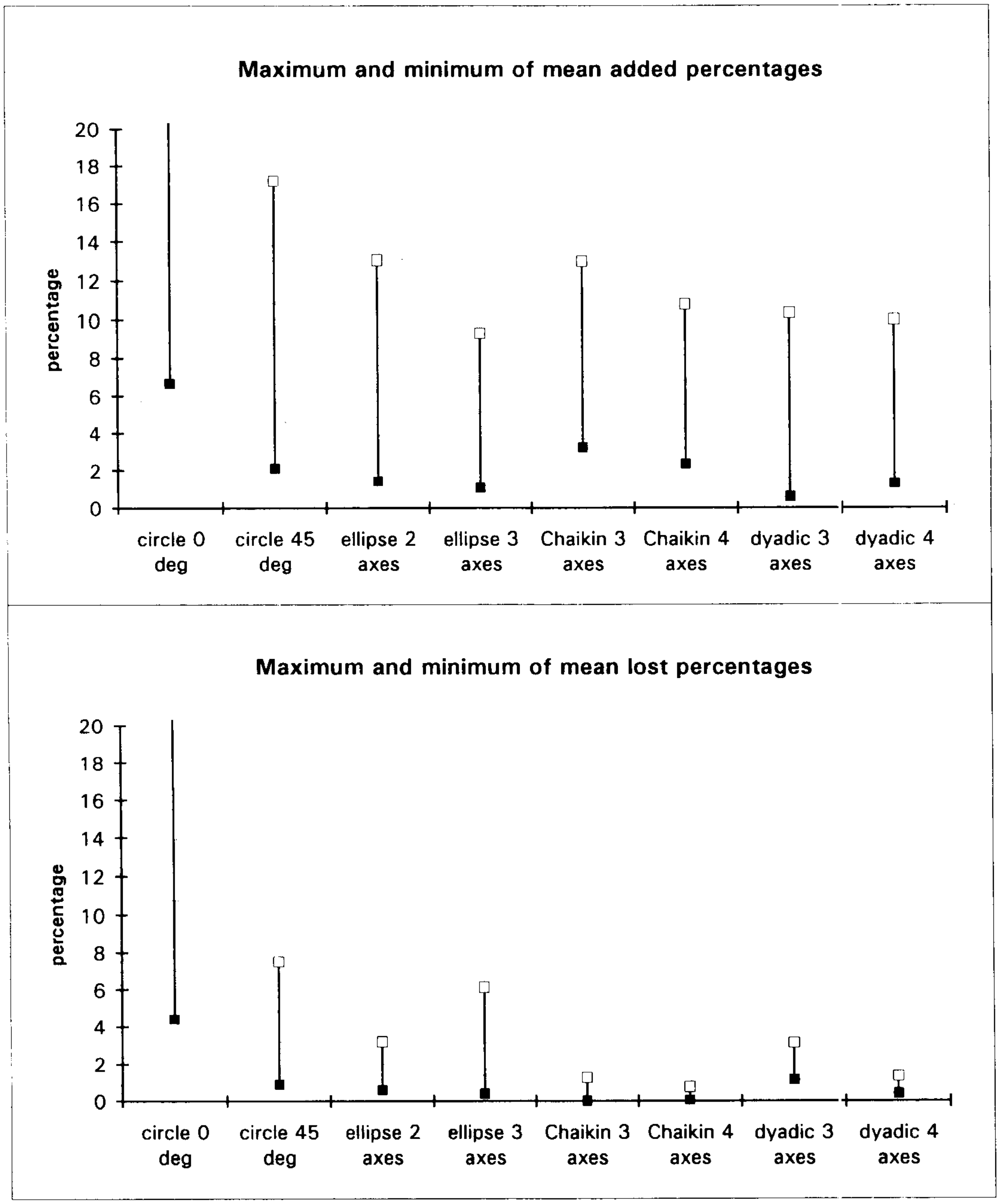

FIG. 13. Overall exactness comparisons among the models were based upon the maximum and minimum errors over all sections (all logs). Each section was represented by the mean lost error and mean added error over all orientations.

surements. Chaikin's and dyadic models produced low lost fiber—under 3.5%—but up to 13% added fiber.

Generally, the studied models overestimate the cross section area. This can be seen on lost and added fiber graphs. The added fiber maximums are higher than lost fiber maximums. The 3-axis ellipse is an exception. Overestimation of section area having the higher effect on lost yield, 3-axis elliptical model may be judged as better than the 2-axis model. The differences between elliptical 3-axis, Chaikin's 4-axis, and dyadic models were small with respect to added fiber. The maximum values were nearly equal. On the lost fiber graph, the variation of maximums was less than 2% between the same models. This variation was small compared to the added fiber maximum (around 11%). The potential increase of exactness with regard to lost fiber by using a 4-axis scanner was hidden by the added percentage maximum.

SUMMARY AND CONCLUSIONS

The horizontally scanned 1-axis circular model demonstrated poor accuracy by all measures. Unable to locate both coordinates of the section center, it provided inconsistent results upon section rotation. The 45°, 1-axis circular model was much more consistent because it was able to find both coordinates at each orientation. Set-of-points models provided more consistent results than the functional models.

No model exhibited excellent flexibility. All models tended to be more exact for stem cross sections than for stump sections, which were more irregular. All 3-axis, 4-axis models—ellipse, Chaikin's, and dyadic—demonstrated comparable flexibility.

Lost fiber has a smaller effect on yield loss (Lewis 1985a). The first objective in log modelling is then to reduce added fiber. However, conclusions about the relative harm of lost and added fiber cannot be made without a study relating combinations of these to lumber volume losses for real logs. The second objective is to increase efficiency sufficiently for real time sawmill processing. The 3-axis elliptical model seems to represent the best function type alternative; functional models are known to be more efficient than set-of-points models. There were only small differences between Chaikin's and dyadic models in the global classification. Exactness was not significantly improved by adding a scanner head to the 3-axis scanners. Dyadic and Chaikin 3-axis models appeared to be the better system choices, although their efficiencies have not been demonstrated.

Almost all models of this study overestimate cross section area. The inability of shadow scanners to detect section concavity explains the big difference between maximum lost percentage and maximum added fiber percentages. If more accuracy is needed, technology other than shadow types is recommended.

REFERENCES

ALLECKSON, T. D., H. B. SANDERS, A. J. KOIVO, AND T. J. WILLIAMS. 1980. Studies on the optimum production of lumber by computer positioning of logs in sawmills. Report number 79, Purdue Laboratory for Applied Industrial Control, Purdue University, Lafayette, IN.

CHAIKIN, G. M. 1974. An algorithm for high speed curve generation. Computer Graphics and Image Processing 3:346–349.

COLEMAN, H. W., AND W. G. STEELE, JR. 1989. Experimentation and uncertainty analysis for engineers. Wiley, New York, NY.

DRAKE, E., AND L. G. JOHANSSON. 1985. Log positioning—A method for evaluating the possible increase of yield. Paper presented at the 8th Wood Machining Seminar, October 1985, Forest Product Laboratory, Richmond, Virginia.

DUBUC, S. 1986. Interpolation through an iterative scheme. J. Math. Anal. Appl. 114(1):185–204.

FUNCK, J. W., A. G. MARISTANY, D. A. BUTLER, AND C. C. BREMER. 1989. Resolution in machine vision—What is it and why is it important? Proceedings of the 3rd International Conference on Scanning Technology in Sawmilling, San Francisco, CA. Pp. XIII-1, XIII-11.

GEERTS, J. M. P. 1984. Mathematical solution for optimising the sawing pattern of a log given its dimensions and its defect core. N.Z. J. Forest. Sci. 14(1):124–134.

HARLESS, E. G. T. 1990. Impact of defect locations on lumber value yield of hardwood logs. Ph.D. dissertation, Mississippi State University, Mississippi State, MS.

HITREC, V., B. MARIJAN, AND K. SEGOTIC. 1990. A model of computer aided optimization of sawing logs. Proceedings of the IUFRO XIX Congrès Mondial, août 1990, Montréal, Canada. Pp. 216–224.

LEBAN, J. M., AND G. DUCHANOIS. 1990. SIMQUA: Un logiciel de simulation de la qualité du bois. Ann. Sci. For. 47:483–493.

LEWIS, D. W. 1985a. Yield losses from sawmill scanner error. Research paper FPL-459, USDA Forest Service, Madison, WI.

———. 1985b. Sawmill simulation and the Best Opening Face System, A user's guide. General Tech. Rep. FPL-48, USDA Forest Service, Madison, WI.

MANESS T. C., AND D. M. ADAM. 1991. The combined optimization of log bucking and sawing strategies. Wood Fiber Sci. 23(2):296–314.

MOEN, D. A. 1991. Three-dimensional profile log scanning and optimization for high recovery and production from small logs. Proceedings of the 4th International Conference on Scanning Technology in the Wood Industry, Burlingame, CA. Pp. Moen-1, Moen-9.

MONGEAU, J. P. 1990. Propriétés de l'interpolation itérative. Ph.D. dissertation, Montréal University, Montreal, Quebec. Canada.

OCCENA, L. G., AND J. M. A. TANCHOCO. 1988. Computer graphics simulation of hardwood log sawing. Forest Prod. J. 38(10):72–76.

RICKFORD, E. N. 1987. Evolution of scanning and computer optimization in sawmilling. Proceedings of the 2nd International Conference on Scanning Technology in Sawmilling, San Francisco, CA. Pp. I-1, I-23.

———. 1989. Scanning for true shape. Proceedings of the 3rd International Conference on Scanning Technology in Sawmilling, San Francisco, CA. Pp. II-1, II-41.

REYNOLDS, H. W. 1970. Sawmill simulation: Data instructions and computer programs. Research Paper NE-152, USDA Forest Service, Northeast Forest Exp. Sta., Princeton, WV.

SAMPSON, S. 1990. Modélisation graphique du débitage du bois. M.Sc. dissertation, Laval University, Quebec, Canada.

TODOKORI, C. L. 1988. SEESAW: A visual sawing simulator, as developed in version 3.0. NZ J. Forest. Sci. 18(1):116–123.

WAGNER F. G., AND F. W. TAYLOR. 1975. Simulated sawing with a chipping headrig. Forest Prod. J. 25(10): 24–28.

ZENG, Y. 1991. Log breakdown using dynamic programming and 3-D log shape. M.Sc. dissertation, Oregon State University, Corvallis, OR.